Dielectric screening in two-dimensional insulators: Implications for excitonic and impurity states in graphane

Pierluigi Cudazzo,[1] Ilya V. Tokatly,[1,2] and Angel Rubio[1,3]

[1]*Nano-bio Spectroscopy Group and European Theoretical Spectroscopy Facility (ETSF) Scientific Development Centre, Departamento Física de Materiales, Universidad del País Vasco/Euskal Herriko Unibertsitatea, Centro de Física de Materiales (CSIC-UPV/EHU-MPC) and Donostia International Physics Center (DIPC), Avenida de Tolosa 72, E-20018 San Sebastián, Spain*

[2]*IKERBASQUE Basque Foundation for Science E-48011, Bilbao, Spain*

[3]*Theory Department, Fritz-Haber-Institut der Max-Planck-Gesellschaft, Faradayweg 4-6, D-14195 Berlin-Dahlem, Germany*

For atomic thin layer insulating materials we provide an exact analytic form of the two-dimensional (2D) screened potential. In contrast to three-dimensional systems where the macroscopic screening can be described by a static dielectric constant, in 2D systems the macroscopic screening is nonlocal (q dependent) showing a logarithmic divergence for small distances and reaching the unscreened Coulomb potential for large distances. The crossover of these two regimes is dictated by 2D layer polarizability that can be easily computed by standard first-principles techniques. The present results have strong implications for describing gap-impurity levels and also exciton binding energies. The simple model derived here captures the main physical effects and reproduces well, for the case of graphane, the full many-body *GW* plus Bethe-Salpeter calculations. As an additional outcome we show that the impurity hole-doping in graphane leads to strongly localized states, which hampers applications in electronic devices. In spite of the inefficient and nonlocal two-dimensional macroscopic screening we demonstrate that a simple $\mathbf{k} \cdot \mathbf{p}$ approach is capable to describe the electronic and transport properties of confined 2D systems.

I. INTRODUCTION

The study of two-dimensional (2D) electronic systems is of great fundamental significance in physics. Atomic thin layers allow to address the role Coulomb interactions in confined geometries.[1] In this context the synthesis of graphene[2] has triggered a huge amount of work in understanding and controlling the properties of this system. In fact due to its unique electronic properties and the low dimensionality, graphene is considered as one of the most promising materials for future carbon-based electronics. Nevertheless, the peculiar gapless ultrarelativistic energy spectrum of graphene[3,4] makes the creation of carbon nanodevices based on *p-n* junctions highly nontrivial. Therefore, transforming graphene into a semiconductor with a conventional electron spectrum keeping its two dimensionality introduced a challenge that has been a major line of research in the last few years. Recently an important step toward graphene electronics has been made with the synthesis of a fully hydrogenated graphene, named graphane,[5] as well as other chemically functionalized graphenelike structures,[6,7] such as fluorinated graphene (or fluorographene).[8] Graphane is a wide band-gap dielectric[9,10] and therefore it may become an important part of nanoelectronic devices as it opens a way to create 2D *p-n* junctions.[11,12] Similarly, single-atomic layers containing hybridized domains of graphene and h-BN have been synthesized[13] and follow a completely different (electronic) phenomenology as compared to high-purity or damaged graphene. Actually, the search for low-dimensional semiconductors is not only focused on graphene and its derivative compounds but it is also moving toward other layered systems, such as MoS_2, WS_2, $MoSe_2$, $MoTe_2$, and BN which can be efficiently dispersed in common solvents and can be deposited as individual flakes or formed into films.[14] In fact, MoS_2 monolayer has been now synthesized.[15,16] Contrarily to the bulk MoS_2, it is a direct gap semiconductor with a band gap[17] of 1.8 eV and could be used as single-layer transistor.[15] Thus, it is important at this point to make a deep analysis of many body effects and in particular of the nature and functional form of the screening in general low-dimensional systems (in particular two-dimensional semiconductors and insulators). In fact, screening effects play a fundamental role in determining the electron dynamics, the exciton binding energy and the effective electron-electron and electron-phonon interactions in the superconducting state. Moreover the screening dictates the optical and transport properties of 2D devices so that knowing its behavior in low-dimensional systems is fundamental also for practical applications.

Although in the past the problem of the screening in low-dimensional systems has been extensively investigated in 2D metals[18] and semiconducting thin films,[19] the focus of this paper will deal with a strict 2D dielectric. In the present work we provide a strict 2D derivation of the macroscopic screening derived by Keldysh as a limiting case of a thin film.[19] We demonstrate that, contrarily to what happens in 3D systems where the macroscopic screening is mapped in a dielectric constant, in 2D systems the macroscopic screening is nonlocal so that in the Fourier space it is described by a **q**-dependent macroscopic dielectric function.

Among the various 2D dielectrics, graphane is not only a promising material for nanodevices application, but also is very interesting by itself. In fact, theoretical works based on first-principles calculations predict localized spin states at hydrogen vacancies,[20] demonstrate the existence of unusual strongly bound charge-transfer excitons,[21] and indicate that doped graphane is probably a high-T_c superconductor.[22] Therefore in the present work we take graphane as the test system to address in detail the influence of the 2D screening

of the Coulomb potential on the excitonic states and impurity levels. Our findings are general in scope and can be applied to any other 2D insulator, such as the ones described above.

The present work is organized as follows. First, we derive in a simple electrostatic model the exact two-dimensional screened potential and compare it with its three-dimensional counterpart. We also provide a very simple and pictorial understanding of that potential in terms of the potential created by a one-dimensional charge distribution whose length is determined by the two-dimensional layer polarizability. The effect of the specific 2D macroscopic screening is illustrated addressing the electronic and optical properties of perfect graphane as well as the electronic levels introduced by hydrogen vacancies in the layer (hole doping). We close the paper with some brief conclusions and perspectives.

II. DIELECTRIC SCREENING IN TWO-DIMENSIONAL INSULATORS

To determine a long wavelength static dielectric response of a general 2D insulator we consider a dielectric sheet of zero thickness at $z = 0$ embedded into vacuum, and subject to an external potential $\phi_{\text{ext}}(\mathbf{r})$. For definiteness we assume that $\phi_{\text{ext}}(\mathbf{r})$ is produced by a point charge placed at the origin $n_{\text{ext}}(\mathbf{r}) = e\delta(\mathbf{r})$. The total electrostatic potential ϕ produced by the external source is related to the total charge density n by Poisson's equation

$$\nabla^2 \phi(\mathbf{r}) = -4\pi n(\mathbf{r}), \tag{1}$$

where $n = n_{\text{ext}} + n_{\text{ind}}$ is the sum of the external charge density and the induced charge density. The induced charge density is confined on the plane $z = 0$ and, in the long wave length limit, is related to the 2D macroscopic polarization $\mathbf{P}_{\text{2D}}$ ($n_{\text{ind}} = -\nabla \cdot \mathbf{P}_{\text{2D}}$), which, in turn is proportional to the in-plane component of the total electric field. Introducing the 2D polarizability α_{2D} of the dielectric sheet, so that $\mathbf{P}_{\text{2D}}(\boldsymbol{\rho}) = -\alpha_{\text{2D}} \nabla_{\boldsymbol{\rho}} \phi(\boldsymbol{\rho}, z = 0)$ we obtain an expression of the induced charge density in terms of the macroscopic potential evaluated at a point $\mathbf{r} = (\boldsymbol{\rho}, z = 0)$

$$n_{\text{ind}}(\mathbf{r}) = \delta(z)\alpha_{\text{2D}} \nabla_{\boldsymbol{\rho}}^2 \phi(\boldsymbol{\rho}, z = 0). \tag{2}$$

With this result for the induced charge density the Poisson equation for the potential of the external point charge takes the form

$$\nabla^2 \phi(\mathbf{r}) = -4\pi e\delta(\mathbf{r}) - 4\pi\alpha_{\text{2D}} \nabla_{\boldsymbol{\rho}}^2 \phi(\boldsymbol{\rho}, z = 0)\delta(z), \tag{3}$$

while its Fourier transform can be written as

$$\left(|\mathbf{q}|^2 + k_z^2\right)\phi(\mathbf{q}, k_z) = 4\pi e - 4\pi\alpha_{\text{2D}}|\mathbf{q}|^2 \underbrace{\int \frac{dk_z}{2\pi}\phi(\mathbf{q}, k_z)}_{\phi_{\text{2D}}(\mathbf{q})}, \tag{4}$$

where $\mathbf{q}$ is the in-plane component of the wave vector, and the k_z integral in the right-hand side defines the Fourier component $\phi_{\text{2D}}(\mathbf{q})$ of the 2D macroscopic potential. By solving Eq. (4) we obtain the following result for $\phi_{\text{2D}}(\mathbf{q})$:

$$\phi_{\text{2D}}(\mathbf{q}) = \frac{2\pi e}{|\mathbf{q}|(1 + 2\pi\alpha_{\text{2D}}|\mathbf{q}|)}, \tag{5}$$

which defines the 2D macroscopic screening of a point charge. As can be seen, for a 2D insulator the macroscopic dielectric

screening is no more described by a simple dielectric constant that renormalizes the electronic charge as in 3D systems. In 2D systems a formally defined dielectric function is intrinsically $\mathbf{q}$ dependent,

$$\epsilon(\mathbf{q}) = 1 + 2\pi\alpha_{\text{2D}}|\mathbf{q}|. \tag{6}$$

By the inverse Fourier transform of $e\phi_{\text{2D}}(\mathbf{q})$, we can determine the effective potential $V_{\text{eff}}(\rho)$, which is felt by an electron living in the 2D dielectric in presence of a point charge

$$V_{\text{eff}}(\rho) = \frac{e^2}{4\alpha_{\text{2D}}}\left[H_0\left(\frac{\rho}{r_0}\right) - Y_0\left(\frac{\rho}{r_0}\right)\right], \tag{7}$$

where H_0 and Y_0 are the Struve function and the second-kind Bessel function, respectively, and $r_0 = 2\pi\alpha_{\text{2D}}$. From the known asymptotic properties of the Struve and Bessel functions[23] we determine the following asymptotic behavior of $V_{\text{eff}}(\rho)$:

$$\lim_{\rho \to \infty} V_{\text{eff}}(\rho) \sim \frac{1}{\rho} \tag{8}$$

$$\lim_{\rho \to 0} V_{\text{eff}}(\rho) \sim -\frac{1}{r_0}\left[\ln\left(\frac{\rho}{2r_0}\right) + \gamma\right], \tag{9}$$

where $\gamma \approx 0.5772$ is the Euler's constant. By the simplest possible matching of the two asymptotic behaviours we can construct an approximated expression for $V_{\text{eff}}(\rho)$ in terms of elementary functions

$$V'_{\text{eff}}(\rho) = -\frac{1}{r_0}\left[\ln\left(\frac{\rho}{\rho + r_0}\right) + (\gamma - \ln 2)e^{-\frac{\rho}{r_0}}\right], \tag{10}$$

which gives an accurate description of the effective interaction also at intermediate values of ρ/r_0 as can be inferred from Fig. 1.

The above results clearly show that, in contrast to the 3D case, the screening in 2D dielectrics introduces a length scale r_0, which is determined by the the polarizability α_{2D} of the dielectric layer. When ρ is larger than r_0 the effective potential behaves like the 3D unscreened Coulomb potential while for $\rho \to 0$ it diverges logarithmically [i.e., it goes like the Coulomb potential in two spatial dimensions (the potential of a charged string)]. Obviously the logarithmic divergence
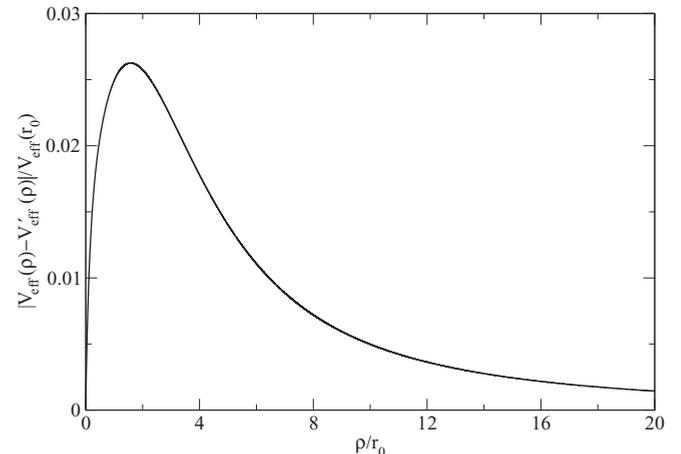
FIG. 1. Comparison between the true effective potential $V_{\text{eff}}(\rho)$ from Eq. (7) and its approximated form $V'_{\text{eff}}(\rho)$ described by Eq. (10).
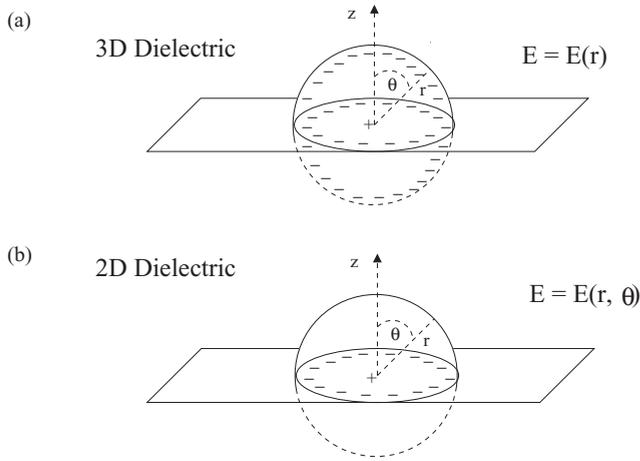
FIG. 2. Schematic representation of the effect of the macroscopic polarization induced by a positive point charge on the $z = 0$ plane in 3D (a) and 2D (b) dielectrics.

weakens when α_{2D} increases, which means that the screening is more efficient in highly polarizable systems.

To better understand the difference of the screening in 3D and 2D insulators we consider a point charge surrounded by a 3D and 2D dielectric medium, respectively [see Figs. 2(a) and 2(b)]. The total electric field ($\mathbf{E}$) at a distance r from the point charge will be the sum of the external field produced by the point charge [$\mathbf{E}_{ext}(\mathbf{r}) = \frac{e}{r^2}\hat{\mathbf{r}}$] and the induced field [$\mathbf{E}_{ind}(\mathbf{r}) = -4\pi\mathbf{P}(\mathbf{r})$]. In 3D dielectrics the latter is equivalent to the electric field produced by a uniform charge distribution on a sphere of radius r centered on the point charge [see Fig. 2(a)]. This charge distribution produces a field of the same functional form as that of the external point charge itself, $\mathbf{E}_{ind}(\mathbf{r}) \sim \mathbf{E}_{ext}(\mathbf{r})$, which means that the screening is given by a simple multiplicative renormalization. In the 2D case the situation is quite different. As can be inferred from Fig. 2(b), since the system is polarizable only on the plane, $\mathbf{E}_{ind}$ is equivalent to the electric field produced by a uniform charge distribution on a circle of radius r. As a consequence it will be a function of r and θ with a functional form substantially different from $\mathbf{E}_{ext}(\mathbf{r})$. This results in a nonlocal macroscopic screening.

A simple and pictorial understanding of the 2D effective potential $V_{eff}(\rho)$ can be obtained by rewriting Eq. (7) in a different form. Starting from Eq. (5) we replace the factor $(1 + 2\pi\alpha_{2D}|\mathbf{q}|)^{-1}$ by its integral representation and rewrite $\phi_{2D}(\mathbf{q})$ as follows:

$$\phi_{2D}(\mathbf{q}) = \int_{-\infty}^{\infty} dz \frac{2\pi e}{|\mathbf{q}|} e^{-|\mathbf{q}||z|} \frac{e^{-\frac{|z|}{2\pi\alpha_{2D}}}}{4\pi\alpha_{2D}}. \tag{11}$$

Performing the Fourier transform we get the following expression for the effective interaction between an electron and an external point charge:

$$V_{eff}(\rho) = \int_{\infty}^{\infty} dz \frac{e^2}{\sqrt{\rho^2 + z^2}} \frac{e^{-\frac{|z|}{r_0}}}{2r_0}. \tag{12}$$

Obviously this equation is absolutely equivalent to Eq. (7), but it is much more clear physically. Indeed, Eq. (12) represents the

potential (in the plane $z = 0$) produced by a one-dimensional charge distribution of the form

$$Q(\mathbf{r}) = e\delta(\boldsymbol{\rho}) \frac{e^{-\frac{|z|}{r_0}}}{2r_0}. \tag{13}$$

Noting that $\int Q(\mathbf{r})d^3\mathbf{r} = e$, we conclude that in the presence of the dielectric plane the point charge produces a field, as it would be effectively smeared out into a 1D string with the charge distribution of Eq. (13). This behavior should be contrasted to the multiplicative renormalization of the charge in 3D dielectrics.

Thus, the effect of the 2D dielectric screening can be visualized as follows: Two electrons living in a 2D dielectric plane interact as two thin charged rods of the length $\sim 2r_0$ and the line charge density $Q(\mathbf{r}) \sim e/2r_0$. The length of the rod sets the characteristic scale of the potential. From large distances $\rho \gg r_0$ the rod is seen as a point charge with the potential given by the classical 3D Coulomb law in Eq. (8). Hence at large distance, the induced polarization is completely inefficient in screening the external field. In the opposite limit $\rho \ll r_0$ the rod looks like an infinite wire with the line charge density $e/2r_0$ so that the effective potential reduces to the classical 2D Coulomb potential of Eq. (9). Thus at small distance the effect of the induced polarization becomes dominant—the $1/r$ singularity is replaced by a weaker logarithmic dependence.

It should be noted that our results for the 2D dielectric screening are very closely related to the results obtained by Keldysh in Ref. 19 for the interaction potential of two point charges in a dielectric slab of the thickness d and characterized by a static bulk dielectric constant ϵ (see also Ref. 24 and references therein). In fact, our Eq. (7) can be recovered in the limit $\rho \gg d$ and $\epsilon \gg 1$.[19] The 1D distribution of the effective charge in Eq. (13) can be also viewed as a limiting form of the discrete image charges used to construct the solution of the electrostatic problem for a finite dielectric slab.[24] The important novel outcome of our derivation is that the form of the effective screened potential of Eq. (7) is valid even for microscopically 2D, atomically thin dielectrics for which the notion of the bulk dielectric constant makes no sense.

The only parameter entering the screened potential of Eqs. (5) and (7) is the polarizability α_{2D} of the 2D dielectric. Let us show how it can be extracted from the standard *ab initio* supercell calculations where 2D systems are simulated using a periodic stack of layers with sufficiently large interlayer distance L. For this auxiliary 3D layered system we can get the 3D macroscopic polarization $P_{3D} = \alpha_{3D}E$, where α_{3D} and E are the 3D polarizability and the total electric field, respectively. The macroscopic 3D polarization can be calculated as an average over N layers in the periodic stack of the microscopic 3D polarization $P_{3D}^{mic}(z)$

$$P_{3D} = \frac{1}{NL} \int dz P_{3D}^{mic}(z), \tag{14}$$

where, in the definition of $P_{3D}^{mic}(z)$ we have already performed the one-layer average. Hence $P_{3D}^{mic}(z)$ can be expressed in terms of the macroscopic 2D polarization $P_{2D} = \alpha_{2D}E_{loc}$ as follows:

$$P_{3D}^{mic}(z) = \sum_{n=0}^{N} P_{2D}\delta(z - nL), \tag{15}$$

with E_{loc} being the local field acting on a single layer. Inserting Eq. (15) in Eq. (14) and taking L sufficiently large so that $E_{\text{loc}} \approx E$ we obtain an expression of α_{2D} in terms of α_{3D} (as a generalized Clausius-Mossotti expression for 2D systems)

$$\alpha_{2D} = L\alpha_{3D} = L\frac{\epsilon - 1}{4\pi}, \tag{16}$$

where ϵ is the static dielectric constant of the 3D layered system. The value of ϵ entering Eq. (16) can be evaluated directly from the first-principles calculation of the dielectric function $\epsilon_{\mathbf{GG'}}(\mathbf{q}, \omega)$ as

$$\epsilon = \lim_{\mathbf{q} \to 0} \frac{1}{[\epsilon^{-1}(\mathbf{q}, \omega = 0)]_{\mathbf{G} = \mathbf{G'} = 0}}. \tag{17}$$

When L goes to infinity, ϵ of the layered system approaches the vacuum dielectric constant, $\epsilon = 1 + O(1/L)$. Therefore the $L \to \infty$ limit of the right-hand side in Eq. (16) yields a finite value that is equal to the 2D polarizability. In practice one performs calculations for several sufficiently large L to ensure the convergence of α_{2D}.

III. EXCITONIC AND IMPURITY STATES IN GRAPHANE

We apply the results of the previous section to the description of excitonic and impurity states in graphane. The problem of excitons in graphane has been addressed recently using a fully *ab initio* many-body self-energy GW plus Bethe-Salpeter equation (GW BSE) approach.[21] In this section we show that the effective screened potential of Eq. (7) combined with the $\mathbf{k} \cdot \mathbf{p}$ description of the electronic and hole states leads to a very simple and accurate description of strongly bound electron-hole and hole-impurity states as obtained from the GW BSE calculations.

Graphane is a representative of wide band gap 2D dielectrics, which is obtained from the ideal graphene by depositing hydrogen atoms on both sides of graphene plane. The resulting electronic structure is dictated by the sp^3 hybridization of the carbon orbitals, which causes the opening of a wide band gap of 5.4 eV (GW value) at the Γ point.[10] States at the top of the valence band belong to E_g 2D irreducible representation of the graphane point group D_{3d}, while the bottom of the conduction band belong to the A_{2u} 1D irreducible representation. As shown in Ref. 21, transitions from the top of the valence band to the bottom of the conduction band are allowed in the dipole approximation and result in strong excitonic effects in the absorption spectra. In particular, the corresponding electron-hole pairs give rise to two nearly degenerate excitons with binding energy of about 1.6 eV. This large binding energy (one order of magnitude larger than in typical semiconductors) seems to be surprising since both valence and conduction bands form almost perfect parabolas in a wide energy-momentum range around the Γ point and therefore the excitonic states are expected to be well described in terms of the effective mass approximation, in spite of their small radius. We will demonstrate explicitly that the effective mass approximation does indeed work perfectly, and that the unusually large binding energy is completely explained by the weak and nonlocal 2D screening discussed in Sec. II.

Let us start with the $\mathbf{k} \cdot \mathbf{p}$ effective mass approximation for the electronic states in graphane.[21,25] The Hamiltonian

for the conduction band is trivially given by $\hat{H}_c(\hat{\mathbf{p}}) = \frac{\hat{p}_x^2 + \hat{p}_y^2}{2m_e}$, while for the valence band Hamiltonian $\hat{H}_v(\hat{\mathbf{p}})$ we adopt the representation obtained in Ref. 25,

$$\hat{H}_v(\hat{\mathbf{p}}) = \tfrac{1}{2}\alpha I\hat{\mathbf{p}}^2 + \tfrac{1}{4}\beta[\sigma_+\hat{p}_+^2 + \sigma_-\hat{p}_-^2], \tag{18}$$

where $\hat{\mathbf{p}} = -i\nabla$ is the in-plane momentum operator, $\hat{p}_\pm = \hat{p}_x \pm i\hat{p}_y$, I is the identity matrix, and $\sigma_\pm = \sigma_x \pm i\sigma_y$ with σ_j being the Pauli matrices, and $\alpha = 2.62/m_0$, $\beta = 0.98/m_0$, and $m_e = 0.83m_0$ are the band parameters expressed in terms of the bare electronic mass m_0 and obtained from the *ab initio* band structures.[21]

The excitonic Hamiltonian for the zero-momentum excitons can then be constructed in standard way[26]

$$\hat{H}_{\text{ex}} = \hat{H}_c(\hat{\mathbf{p}}) + \hat{H}_v(\hat{\mathbf{p}}) - V_{\text{eff}}(\rho), \tag{19}$$

where $V_{\text{eff}}(\rho)$ is the effective 2D screened electron-hole interaction given by Eq. (7). Explicitly the final effective mass equation for the relative motion of the electron and the hole takes the following form:

$$\left[\tfrac{1}{2}\gamma_1\hat{I}\hat{\mathbf{p}}^2 + \tfrac{1}{4}\gamma_2(\hat{\sigma}_+\hat{p}_+^2 + \hat{\sigma}_-\hat{p}_-^2) - V_{\text{eff}}(\rho)\right]\hat{\Phi}(\boldsymbol{\rho}) = E\hat{\Phi}(\boldsymbol{\rho}), \tag{20}$$

where $\gamma_1 = \alpha + \frac{1}{2m_e}$ and $\gamma_2 = \beta$.

To classify the eigenstates of Eq. (20) we note that the Hamiltonian $\hat{H}_{\text{ex}}$ commutes with an operator $\hat{L}_z$ that is defined as follows:

$$\hat{L}_z = (\boldsymbol{\rho} \times \hat{\mathbf{p}})_z - \sigma_z \equiv (x\hat{p}_y - y\hat{p}_x) - \sigma_z. \tag{21}$$

Obviously, the operator $\hat{L}_z$ corresponds to the z component of the total angular momentum, with the second term in Eq. (21) being related to the orbital momentum of the local currents inside the unit cell of graphane.[25] Since $[\hat{H}_{\text{ex}}, \hat{L}_z] = 0$ the excitonic states can be classified by the eigenstates of the total angular momentum operator. In other words, the eigenfunctions of Eq. (20) can be written in terms of radial wave functions $[\mathcal{Z}_l(\rho), \chi_l(\rho)]$ ordered by the integer quantum number l defining the eigenvalue of $\hat{L}_z$

$$\hat{\Phi}_l(\rho, \theta) = \begin{pmatrix} e^{i\theta}\mathcal{Z}_l(\rho) \\ e^{-i\theta}\chi_l(\rho) \end{pmatrix}e^{il\theta}. \tag{22}$$

Inserting the expression of Eq. (22) into Eq. (20) we obtain the equation for the radial part of the envelope wave functions

$$\left[-\frac{\gamma_1}{2}\left(\partial_\rho^2 + \frac{1}{\rho}\partial_\rho - \frac{(1+l)^2}{\rho^2}\right) - V_{\text{eff}}(\rho)\right]\mathcal{Z}_l(\rho)$$
$$-\frac{\gamma_2}{2}\left(\partial_\rho - \frac{l}{\rho}\right)\left(\partial_\rho + \frac{1-l}{\rho}\right)\chi_l(\rho) = E_l\mathcal{Z}_l(\rho), \tag{23}$$

$$\left(-\frac{\gamma_1}{2}\left[\partial_\rho^2 + \frac{1}{\rho}\partial_\rho - \frac{(1-l)^2}{\rho^2}\right] - V_{\text{eff}}(\rho)\right)\chi_l(\rho)$$
$$-\frac{\gamma_2}{2}\left(\partial_\rho + \frac{l}{\rho}\right)\left(\partial_\rho + \frac{1+l}{\rho}\right)\mathcal{Z}_l(\rho) = E_l\chi_l(\rho). \tag{24}$$

Thus, each excitonic state is completely defined by the quantum number l and the positive integer n denoting the discrete eigenvalues of Eqs. (23) and (24) for given l.

The corresponding microscopic wave function of the exciton for a fixed position $\mathbf{r}_h$ of the hole can be written as follows:

$$\Psi_{ex}^l(\mathbf{r},\mathbf{r}_h) = \mathcal{Z}_l(\boldsymbol{\rho})\psi_e(\mathbf{r})\psi_h^{(1)}(\mathbf{r}_h) + \chi_l(\boldsymbol{\rho})\psi_e(\mathbf{r})\psi_h^{(2)}(\mathbf{r}_h),$$

(25)

where ψ_e is the electron Bloch wave function and $\psi_h^{(1,2)}$ the hole Bloch wave functions related to the twofold degenerate valence bands.

Analyzing the structure of Eqs. (23) and (24), we observe that for all $l \neq 0$ the system of differential equations is invariant under the transformation $l \to -l$, $\mathcal{Z} \to \chi$, $\chi \to \mathcal{Z}$. Therefore all excitonic states with $l \neq 0$ are double degenerate with $E_l = E_{-l}$, which is a clear consequence of the time-reversal invariance of the Hamiltonian. We also note that only excitons corresponding to $l = \pm 1$ are dipole active.

The only nondegenerate state corresponds to a dark exciton with zero angular momentum, $l = 0$. Interestingly, for $l = 0$ the diagonal and off-diagonal operators in the system of Eqs. (23) and (24) are equal to each other. As a results the problem reduces to completely decoupled equations for the symmetric and antisymmetric states

$$\left[-\frac{1}{2}(\gamma_1 \pm \gamma_2)\left(\partial_\rho^2 + \frac{1}{\rho}\partial_\rho - \frac{1}{\rho^2}\right) - V_{eff}(\rho)\right]\phi_\pm(\rho) = E_\pm \phi_\pm(\rho)$$

(26)

and the excitonic spinor wave function for $l = 0$ takes the form

$$\hat{\Phi}_{l=0}^\pm = \frac{1}{\sqrt{2}}\begin{pmatrix} e^{i\theta}\phi_\pm \\ e^{-i\theta} \pm \phi_\pm \end{pmatrix}.$$

(27)

To practically solve Eqs. (23) and (24) we expanded the radial part of the envelope wave function on the 2D hydrogen eigenfunctions $u_{n,l}$,[27] so that $\mathcal{Z}_l(\rho) = \sum_n a_n u_{n,l+1}(\rho)$ and $\chi_l(\rho) = \sum_n b_n u_{n,l-1}(\rho)$. This complete orthonormal basis set assures the correct asymptotic behavior of the eigenfunctions of the excitonic Hamiltonian.

Our results for a selected set of lowest-energy states are summarized in Table I. As we can see, the ground state of the excitonic Hamiltonian corresponds to $l = \pm 1$. This state is twofold degenerate and optically active with the binding energy $E_{l=\pm 1} = 1.77$ eV, which is in a perfect agreement with the values obtained by solution of the Bethe-Salpeter equation.[21] The corresponding excitonic wave

TABLE I. Exciton binding energy and impurity levels in the effective mass approximation for some selected values of the quantum numbers n and l.

Angular momentum (l)	Quantum number (n)	Exciton energy (eV)	Impurity level (eV)
$l = \pm 1$	$n = 1$	-1.77	-2.12
	$n = 2$	-0.67	-0.90
$l = 0$	$n = 1$	$E_+ = -1.13$	$E_+ = -1.47$
		$E_- = -0.78$	$E_- = -0.92$
	$n = 2$	$E_+ = -0.52$	$E_+ = -0.74$
		$E_- = -0.34$	$E_- = -0.45$
$l = \pm 2$	$n = 1$	-0.92	-1.17
	$n = 2$	-0.43	-0.58
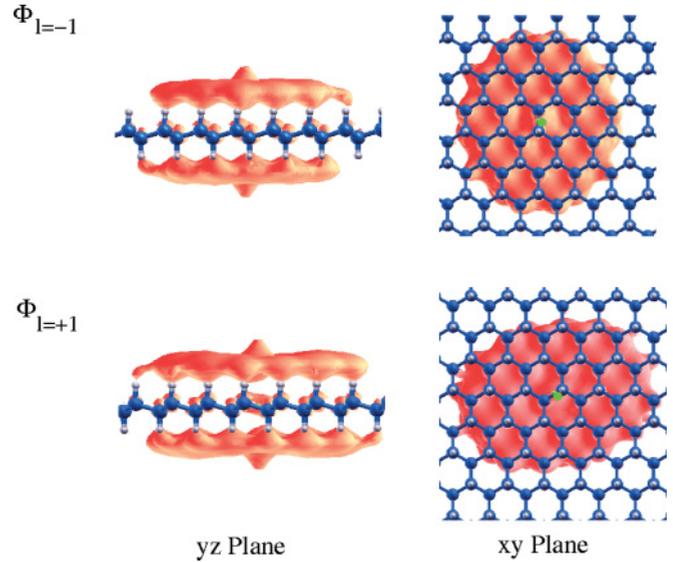
FIG. 3. (Color online) 3D shape of the low-energy excitonic wave functions for a fixed position of the hole (marked as a green circle) as obtained from Eq. (25). Note that the shape of the excitonic wave functions is in perfect agreement with that obtained by the full solution of the BS equation in Ref. 21.

functions (Fig. 3), calculated using Eq. (25), show that both excitons are strongly localized with an average radius of about 11.5 a.u. As can be inferred from Fig. 3 these excitations give rise to a charge transfer from the carbon plane toward the hydrogen plane that corresponds to 0.5 e^-. The first excited state corresponds to zero angular momentum $l = 0$. This dark exciton is also found from the solution of the Bethe-Salpeter equation, which is additional confirmation of the present simple theory.

Therefore our results demonstrate that, despite the large binding energy, excitons in graphane are indeed described in terms of the effective mass approximation, provided the correct form of the effective electron-hole interaction is used [as derived in the present work, Eqs. (7) and (12)]. We clearly see that the unusual, large binding energy is related to a weak and nonlocal 2D dielectric screening that is completely inefficient at large distances. The small overestimation of the exciton binding energy with respect to the *ab initio* value may be ascribed to the lack in our approach of short-range contributions to the induced polarization and exchange electron-hole interaction. All these effects can only reduce the exciton binding energy. As a matter of fact, the effects of short-range corrections are small and, if necessary, can be easily included perturbatively. We emphasize that our model also describes the strong excitonic effects found on recently synthesized fluorographene[8] (with the appropriate values of γ_1, γ_2, and α_{2D}). In fact this system presents a band structure close to that of graphane with the top of valence band and the bottom of the conduction band belonging to the E_g and A_{2u} irreducible representation of the D_{3d} point group respectively.[8] This assures that valence and conduction bands in graphane and fluorographene can be described using the same $\mathbf{k} \cdot \mathbf{p}$ Hamiltonian.

Using the same formalism we can now look at the effect of the 2D screening on impurity states. First, we focus on the acceptor states in the hole-doped graphane, as it is expected

to be the most natural way to dope this system. Indeed, one may assume that extra holes are easily introduced by dehydrogenation.

Similarly to the excitonic case, the parabolicity of the valence bands in a wide energy range suggests that holes in the presence of hydrogen vacancies can be well described in terms of the effective mass approximation. Therefore acceptor impurity levels can be obtained by solving Eqs. (23) and (24) with $\gamma_1 = \alpha$. The corresponding results are presented in Table I. The ground impurity state corresponds to $n = 1$ and $l = \pm 1$ and is characterized by a binding energy of about 2.12 eV in good agreement with the *ab initio* value (1.86 eV). This quantity represents the position of the impurity level with respect to the top of the valence band. Therefore, for impurity levels the 2D nonlocal screening results in unusually large binding energy that exceeds by two or three orders of magnitude the corresponding values for typical semiconductors, a result found also in graphane nanoribbons[28] and flakes.[29] Comparing the values of the binding energy with the gap energy (5.4 eV) we find that the impurity level is close to the center of the graphane gap.

Finally, when the dopant is a donor, the electron in the conduction band is described by a simple 2D hydrogen-like Schrödinger equation with $V_{\mathrm{eff}}(\rho)$ of Eq. (7) replacing the Coulomb potential. In this case for the lowest bound state (corresponding to $n = 1$ and $l = 0$) we get a binding energy of about 3.15 eV. Therefore for electron-doped graphane the specific 2D screening of the impurity potential also causes the formation of midgap impurity levels.

The above results lead us to an unfortunate but important conclusion. The standard for 3D semiconductors' impurity doping, both donor and acceptor, will probably not work for graphane and most likely for other atomically thin dielectrics. In particular a slightly dehydrogenated graphane cannot be considered as a semiconductor with extra highly mobile holes in the valence band. All holes will be strongly localized on the hydrogen vacancies with the radius of the bound state of the order of the interatomic distance. The reason for this behavior is a very weak and inefficient screening in 2D dielectric materials.

IV. CONCLUSIONS

In conclusion, we derived an expression of the macroscopic screening in 2D dielectrics showing that, contrary to what happens in 3D systems where the macroscopic screening is mapped in a dielectric constant, in 2D systems the macroscopic screening is nonlocal. As a result the effective potential produced by an external point charge surrounded by a 2D dielectric has a functional form that is substantially different from the bare Coulomb potential. It presents a logarithmic divergence for $\rho \to 0$ and reduces to the unscreened Coulomb potential at large distances. The 2D polarizability α_{2D} determines the characteristic length scale r_0 at which the two asymptotic forms are matched. This behavior strongly modifies the optical and transport properties of 2D systems. In particular we show that hole impurity doping leads to strongly bound localized states with low mobility. Moreover, in spite of the inefficient and two-dimensional macroscopic **q**-dependent screening the simple **k** · **p** approach works very well to describe the electronic properties up to very high energy and very short spatial scales. Our results imply that the **k** · **p** theory supplemented with a proper macroscopic treatment of the 2D screening forms a solid basis for a quantitative description of various, both equilibrium and nonequilibrium, in particular transport, properties of nanostructured 2D systems.

[1] E. Abrahams, S. V. Kravchenko, and M. P. Sarachik, Rev. Mod. Phys. **73**, 251 (2001).

[2] K. S. Novoselov, A. K. Geim, S. V. Morozov, D. Jiang, Y. Zhang, S. V. Dubonos, I. V. Grigorieva, and A. A. Firsov, Science **306**, 666 (2004).

[3] M. I. Katsnelson, Mater. Today **10**, 20 (2007).

[4] A. H. Castro Neto, F. Guinea, N. M. R. Peres, K. S. Novoselov, and A. K. Geim, Rev. Mod. Phys. **81**, 109 (2009).

[5] D. C. Elias, R. R. Nair, T. M. G. Mohiuddin, S. V. Morozov, P. Blake, M. P. Halsall, A. F. Ferrari, D. W. Boukhvalov, M. I. Katsnelson, A. K. Geim, and K. S. Novoselov, Science **323**, 610 (2009).

[6] G. Eda and M. Chhowalla, Adv. Mater. **22**, 2392 (2010).

[7] S.-H. Cheng, K. Zou, F. Okino, H. R. Gutierrez, A. Gupta, N. Shen, P. C. Eklund, J. O. Sofo, and J. Zhu, Phys. Rev. B **81**, 205435 (2010).

[8] D. K. Samarakoon, Z. Chen, C. Nicolas, and X. Q. Wang, Small **7**, 965 (2011).

[9] J. O. Sofo, A. S. Chaudhari, and G. D. Barber, Phys. Rev. B **75**, 153401 (2007).

[10] S. Lebégue, M. Klinterberg, O. Eriksson, and M. I. Katsnelson, Phys. Rev. B **79**, 245117 (2009).

[11] G. Fiori, S. Lebègue, A. Betti, P. Michetti, M. Klintenberg, O. Eriksson, and G. Iannaccone, Phys. Rev. B **82**, 153404 (2010).

[12] B. Gharekhanlou and S. Khorasani, IEEE Transactions on Electron Devices **57**, 209 (2010).

[13] L. J. Ci *et al.*, Nat. Mater. **9**, 430 (2010); A. Rubio, *ibid.* **9**, 379 (2010).

[14] J. N. Coleman, M. Lotya, A. O'Neill, S. D. Bergin, P. J. King, U. Khan, K. Young, A. Gaucher, S. De, R. J. Smith, I. V. Shvets, S. K. Arora, G. Stanton, H.-Y. Kim, K. Lee, G. T. Kim, G. S. Duesberg, T. Hallam, J. J. Boland, J. J. Wang, J. F. Donegan, J. C.

Grunlan, G. Moriarty, A. Shmeliov, R. J. Nicholls, J. M. Perkins, E. M. Grieveson, K. Theuwissen, D. W. McComb, P. D. Nellist, and V. Nicolosi, Science **331**, 568 (2011).

[15] B. Radisavljevic, A. Radenovic, J. Brivio, V. Giacometti, and A. Kis, Nature Nanotechnology **6**, 147 (2010).

[16] A. Splendiani, L. Sun, Y. Zhang, T. Li, J. Kim, C. Y. Chim, G. Galli, and F. Wang, Nano Lett. **10**, 1271 (2010).

[17] K. F. Mak, C. Lee, J. Hone, J. Sham, and T. F. Hoinz, Phys. Rev. Lett. **105**, 136805 (2010).

[18] T. Ando, Rev. Mod. Phys. **54**, 437 (1982).

[19] L. V. Keldysh, JETP Lett. **29**, 658 (1978).

[20] H. Sahin, C. Ataca, and S. Ciraci, Appl. Phys. Lett. **95**, 222510 (2009).

[21] P. Cudazzo, C. Attacalite, I. V. Tokatly, and A. Rubio, Phys. Rev. Lett. **104**, 226804 (2010).

[22] G. Savini, A. C. Ferrari, and F. Giustino, Phys. Rev. Lett. **105**, 037002 (2010).

[23] Handbook of Mathematical Functions With Formulas, Graphs, and Mathematical Tables, edited by M. Abramowitz and I. A. Stegun, NBS Applied Mathematics Series 55 (National Bureau of Standards, Washington, 1964).

[24] D. Jena and A. Konar, Phys. Rev. Lett. **98**, 136805 (2007).

[25] I. V. Tokatly, Phys. Rev. B **82**, 161404(R) (2010).

[26] F. Bassani and G. Pastori Parravicini, Electronic States and Optical Transitions in Solids, (Pergamon Press, Oxford, 1975).

[27] X. L. Yang, S. H. Guo, F. T. Chan, K. W. Wong, and W. Y. Ching, Phys. Rev. A **43**, 1186 (1991).

[28] H. Sahin, C. Ataca, and S. Ciraci, Phys. Rev. B **81**, 205417 (2010).

[29] J. Barashevich and T. Chakraborty, Nanotechnology **21**, 355201 (2010).